Supporting Information

An Electronegative Modified Separator with Semi-Fused Pores as Selective Barrier for Highly Stable Lithium–Sulfur Batteries

Junxiao Wang,[a] Mengjia Li,[b] Chong Liu,[a] Yong Liu,[c] Tongkun Zhao,[a] Pengfei Zhai,[a] Jingtao Wang*[a]*

[a] School of Chemical Engineering and Energy, Zhengzhou University, Zhengzhou 450001, P. R. China

[b] School of Materials Science and Engineering, Zhengzhou University, Zhengzhou 450001, P. R. China

[c] National Center for Research & Popularization on Calcium, Magnesium, Phosphate and Compound Fertilizer Technology, Zhengzhou 450001, P. R. China

*To whom correspondence should be addressed.
Fax: +86-371-63887135; Tel: +86-371-63887135;
E-mail: yongliu@zzu.edu.cn(Y. Liu) and jingtaowang@zzu.edu.cn (J.T. Wang)

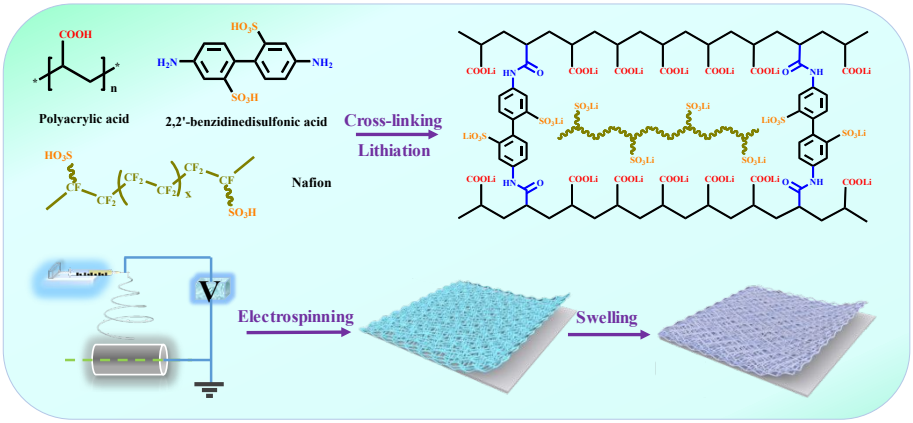

Scheme S1. Schematic illustration of the fabrication process of the NP-Li/PP separator.

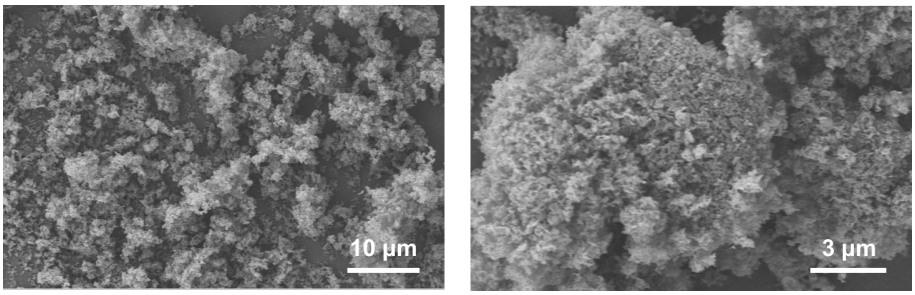

Figure S1. SEM images of CB/S composite at different magnifications.

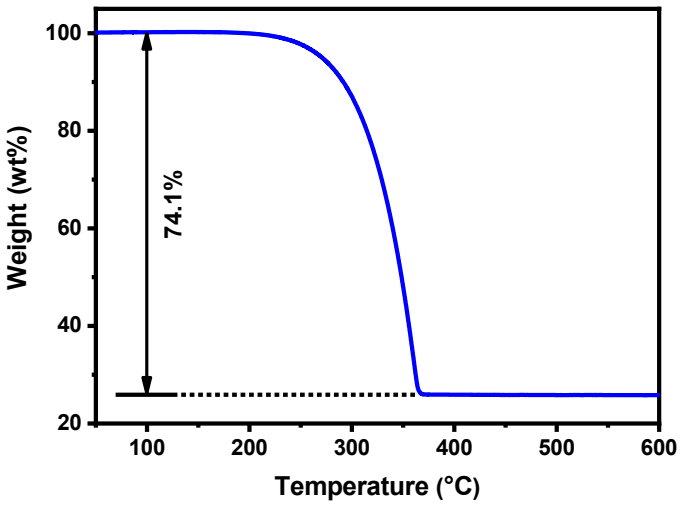

Figure S2. TGA curve of the CB/S composite.

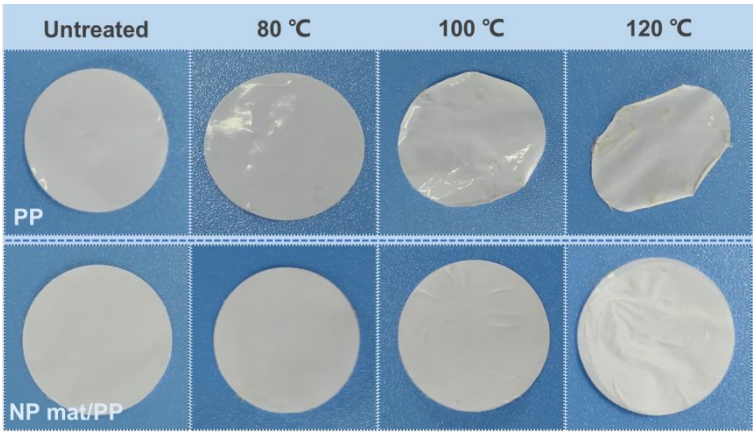

Figure S3. The thermal dimensional stability of separators at different temperatures.

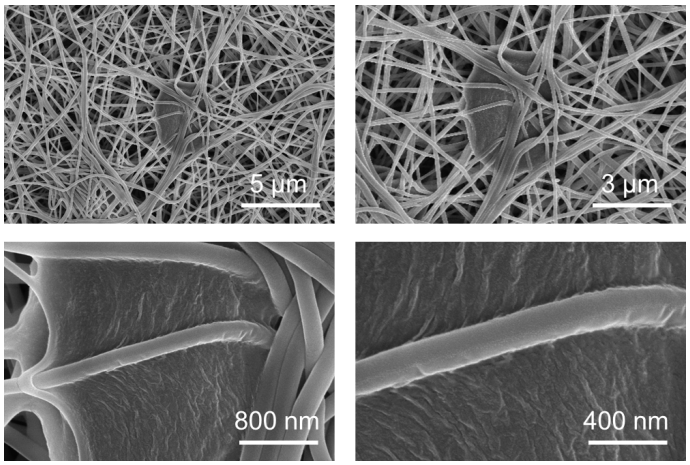

Figure S4. SEM images of local swelling of Nafion/PAA nanofiber at different magnifications.

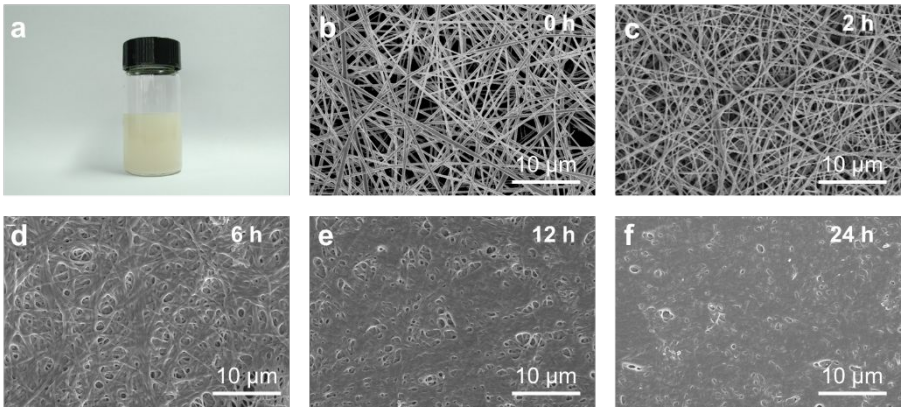

Figure S5. (a) Digital photograph of Nafion/PAA spinning solution. (b) SEM image of pristine NP mat/PP separator. SEM images of NP-Li/PP separators after (c) 2 h, (d) 6 h, (e) 12 h, and (f) 24 h of lithiation.

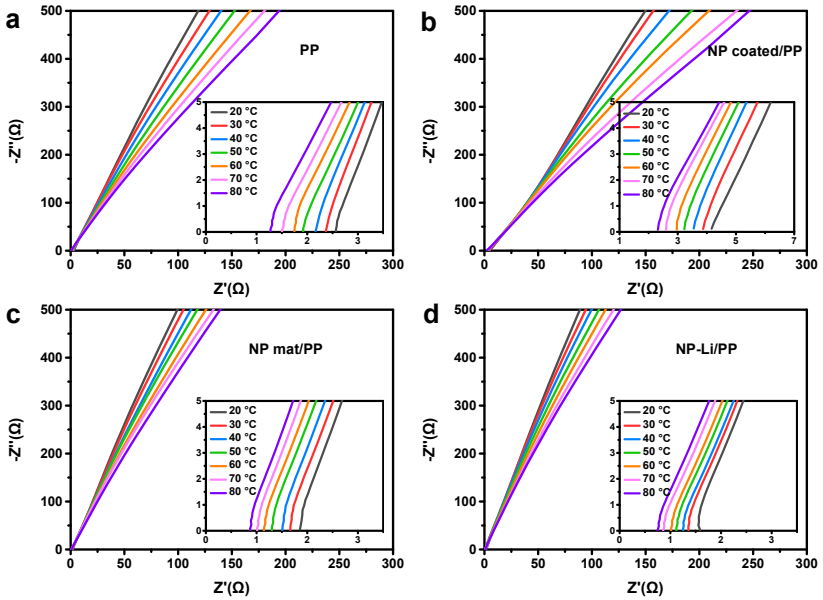

Figure S6. The impedance plots of (a) PP, (b) NP coated/PP, (c) NP mat/PP, and (d) NP-Li/PP separators at different temperatures.

The Li^+ conductivity (σ) was calculated according to the following equation:

$$\sigma = \frac{L}{RA}$$

where R was the separator resistance obtained from the impedance plot, L was the thickness of separator, and A was the area of separator.

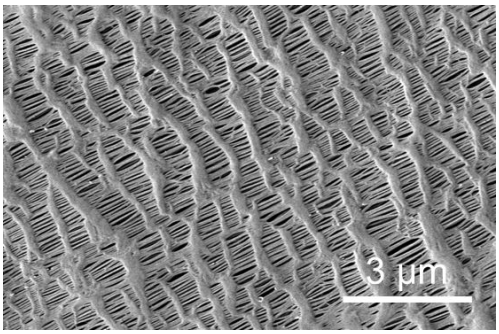

Figure S7. SEM image of PP separator with porous structure.

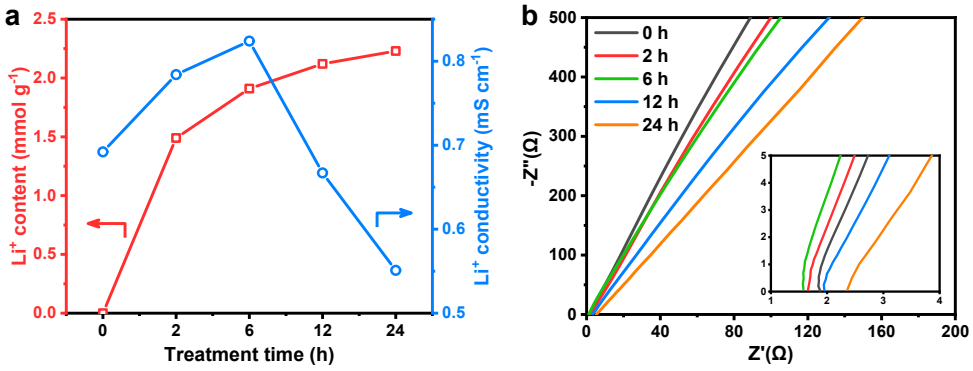

Figure S8. (a) The Li^+ contents, Li^+ conductivities and (b) impedance plots of separators with different treatment times at room temperature.

The Li^+ content (C_{Li^+}) was calculated according to the following equation:

$$C_{Li^+} = \frac{V'_{NaOH}\, c_{NaOH}}{W'} - \frac{V_{NaOH}\, c_{NaOH}}{W}$$

where V'_{NaOH} was the volume of NaOH solution used to titrate untreated modification layer, c_{NaOH} was the molar concentration of NaOH solution, W' was the weight of the untreated modification layer, V_{NaOH} was the volume of NaOH solution used to titrate the modification layer with certain lithiation degree, and W was the weight of the corresponding modification layer.

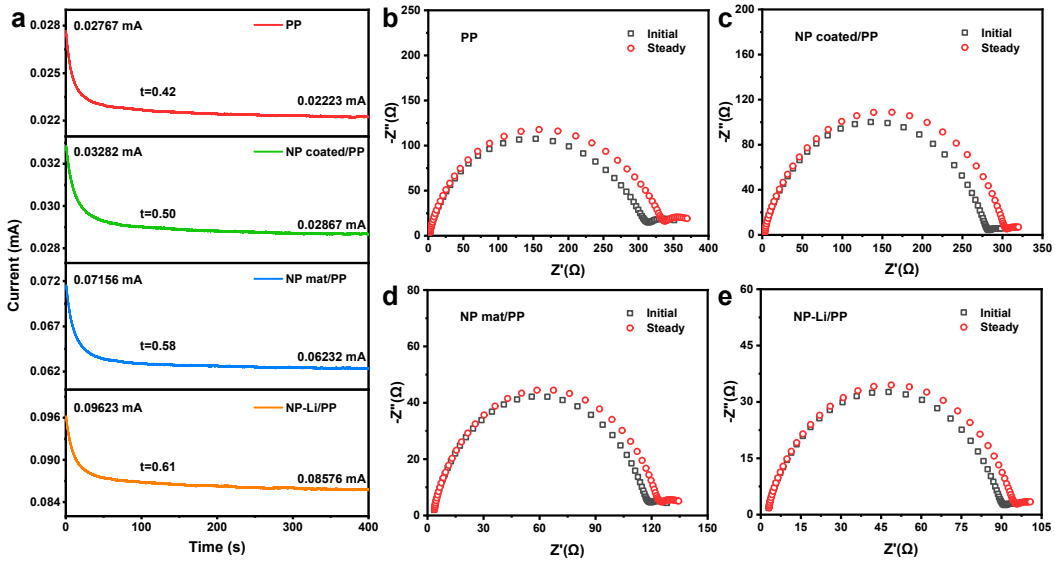

Figure S9. Li^+ transference number of separators. (a) Chronoamperometry profiles, and the impedance plots at initial and steady states for (b) PP, (c) NP coated/PP, (d) NP mat/PP, and (e) NP-Li/PP separators.

The Li^+ transference number (t_{Li^+}) was calculated according to the equation:

$$t_{Li^+} = \frac{I_s(\Delta V - I_0 R_0)}{I_0(\Delta V - I_s R_s)}$$

where I_0 and I_S were the initial and steady-state current obtained from chronoamperometry, respectively, R_0 and R_S were the interfacial resistance before and after polarization, respectively, and ΔV was the potential difference.

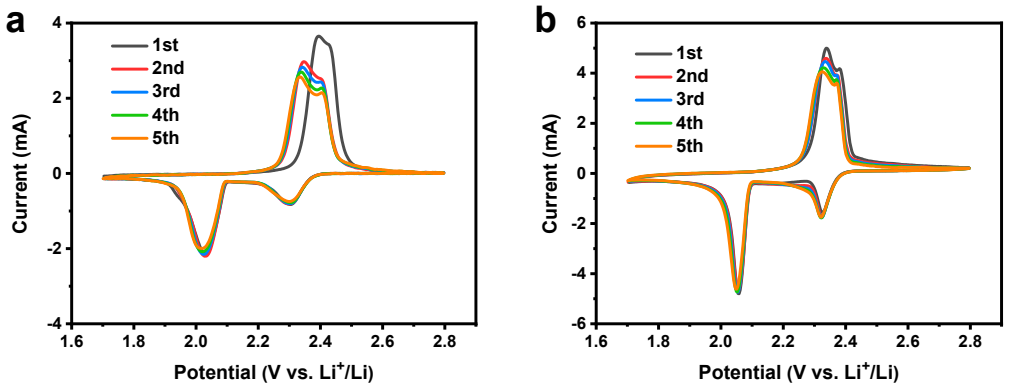

Figure S10. CV curves of the cells with (a) PP and (b) NP-Li/PP separator for the first five cycle.

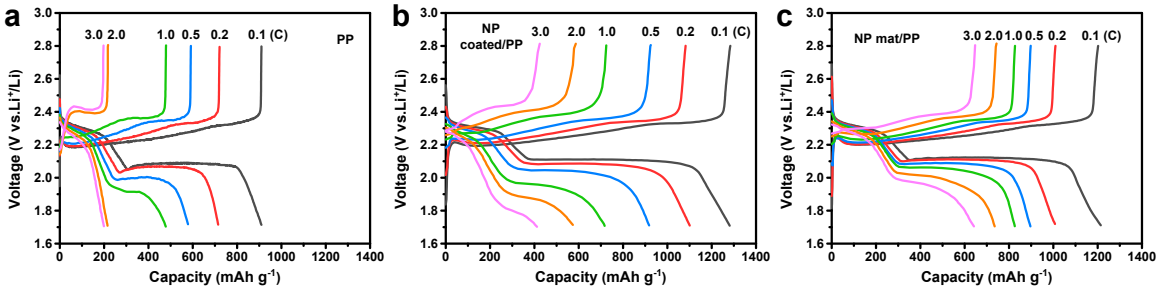

Figure S11. Charge/discharge profiles of the cells with (a) PP, (b) NP coated/PP, and (c) NP mat/PP separators at various rates.

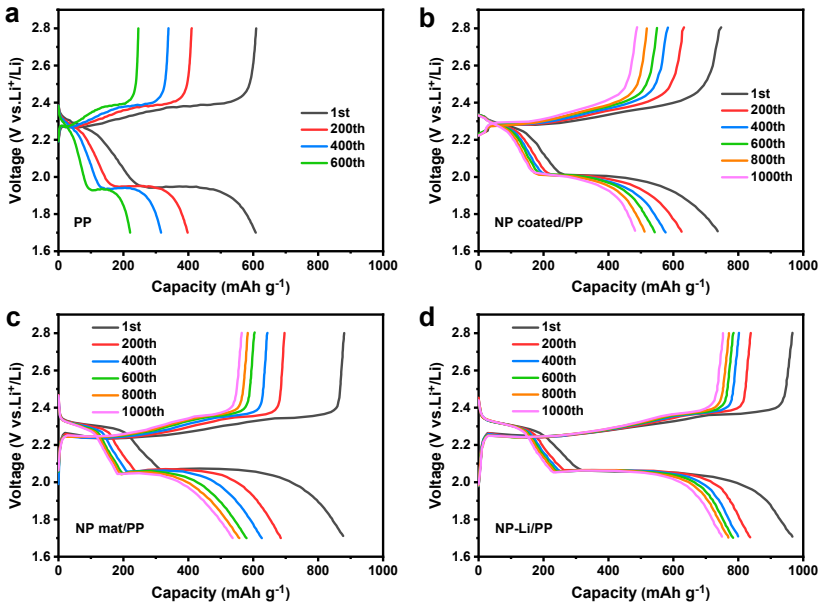

Figure S12. Charge/discharge profiles of the cells with (a) PP, (b) NP coated/PP, (c) NP mat/PP, and (d) NP-Li/PP separators at 1.0 C.

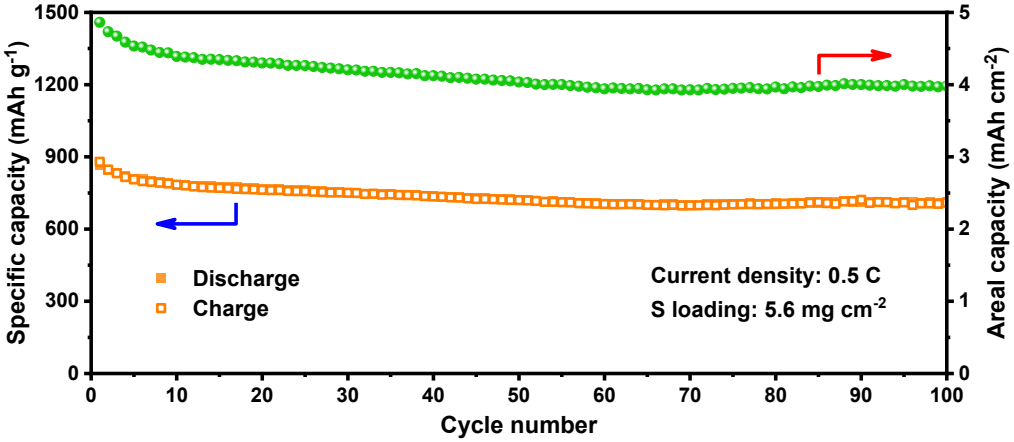

Figure S13. Cycling performance of the cell with NP-Li/PP separator at a high sulfur loading of 5.6 mg cm^{-2}.

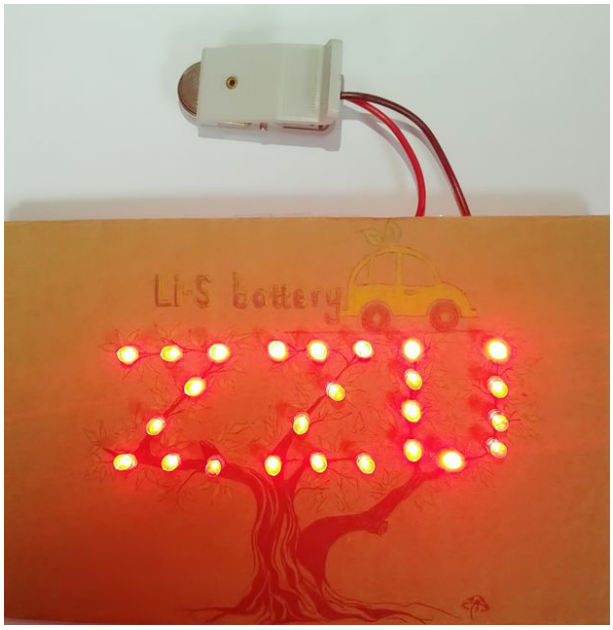

Figure S14. Digital photograph of a homemade light-emitting diode panel lighted by a cell with NP-Li/PP separator.

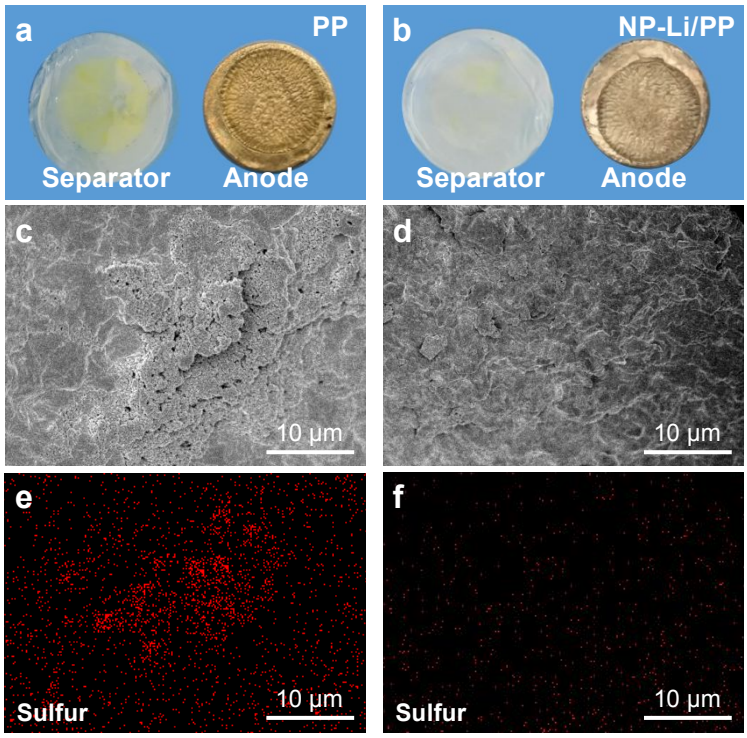

Figure S15. Photographs of disassembled cells with (a) PP and (b) NP-Li/PP separators after long-term cycling test. The top sides of these separators were faced toward cathodes. Surface SEM images of the cycled Li anodes in cells with (c) PP and (d) NP-Li/PP separators. Corresponding sulfur elemental maps of the cycled Li anodes in cells with (e) PP and (f) NP-Li/PP separators.

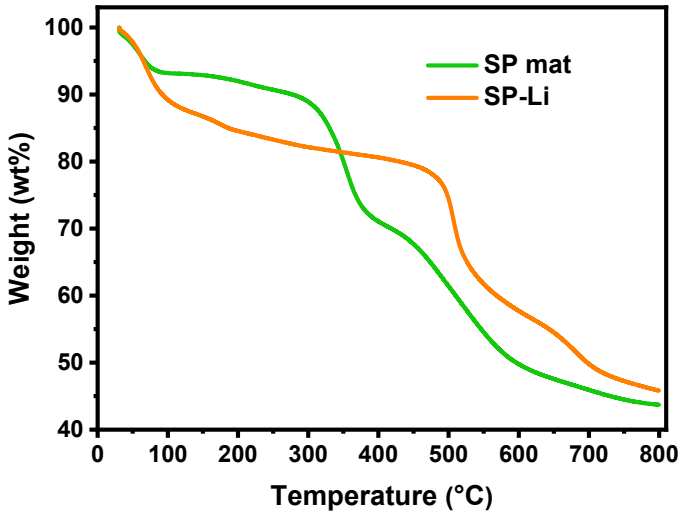

Figure S16. TGA curves of the SP mat and SP-Li.

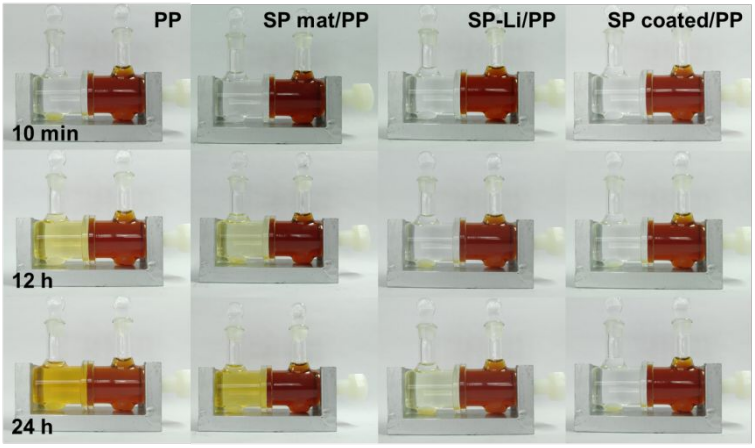

Figure S17. Diffusion of the polysulfides in the U-shaped glass bottles with SPEEK-modified separators.

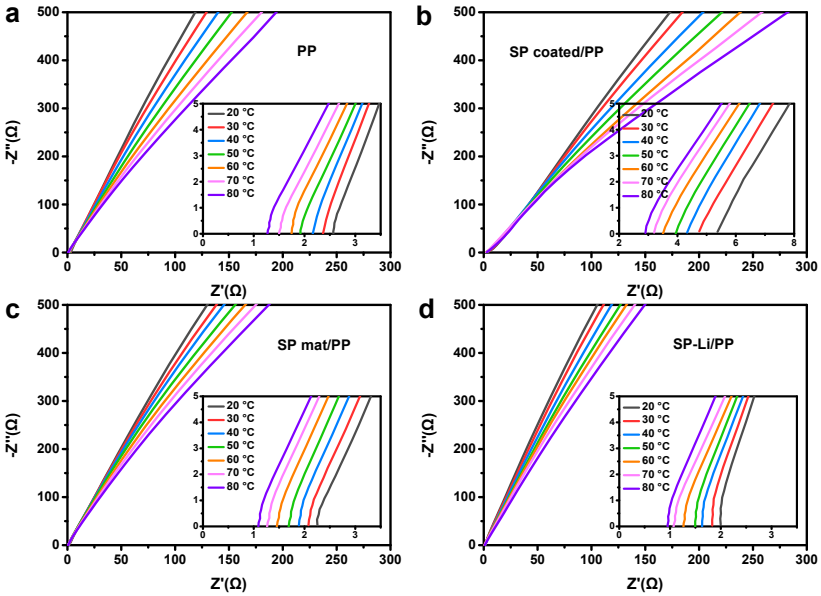

Figure S18. The impedance plots of (a) PP, (b) SP coated/PP, (c) SP mat/PP and (d) SP-Li/PP separators at different temperatures.

Table S1. Comparison of the cycling stability for Li–S batteries with various modified separators.

Barrier	S loading (mg cm^{-2})	S content (wt%)	Rate (C)	Cycle number	Residual capacity (mAh g^{-1})	Cyclic decay rate	Ref.
Nafion	0.5	50	1.0	500	487	0.080	(1)
SPEEK/Nafion composite	6.0	45	0.2	500	650	0.100	(2)
Gum Arabic/carbon nanofiber	1.1	60	1.0	250	827	0.024	(3)
Porphyrin-derived graphene	1.0	63	0.5	300	798	0.099	(4)
Activated carbon nanofiber	2.2	70	0.2	200	819	0.130	(5)
Laponite/carbon black	1.1	70	0.2	500	838	0.060	(6)
Black phosphorus	1.7	67	0.2	100	800	0.139	(7)
Carbon nitride phosphorus	3.2	80	0.5	700	850	0.041	(8)
Carbon/tungsten disulfide	1.5	70	2.0	1000	430	0.046	(9)
Nafion/PAA nanofiber	2.0	74	1.0	1000	748	0.023	This work

SUPPLEMENTARY REFERENCES

(1) Huang, J. Q.; Zhang, Q.; Peng, H. J.; Liu, X. Y.; Qian, W. Z.; Wei, F.; Ionic Shield for Polysulfides towards Highly-Stable Lithium–Sulfur Batteries. *Energy Environ. Sci.* **2014**, *7*, 347.

(2) Babu, D. B.; Giribabu, K.; Ramesha, K. Permselective SPEEK/Nafion Composite-Coated Separator as a Potential Polysulfide Crossover Barrier Layer for Li-S Batteries. *ACS Appl. Mater. Interfaces* **2018**, *10*, 19721.

(3) Tu, S.; Chen, X.; Zhao, X.; Cheng, M.; Xiong, P.; He, Y.; Zhang, Q.; Xu, Y. A Polysulfide-Immobilizing Polymer Retards the Shuttling of Polysulfide Intermediates in Lithium–Sulfur Batteries. *Adv. Mater*. **2018**, *30*, 1804581.

(4) Kong, L.; Li, B. Q.; Peng, H. J.; Zhang, R.; Xie, J.; Huang, J. Q.; Zhang, Q. Porphyrin-Derived Graphene-

Based Nanosheets Enabling Strong Polysulfide Chemisorption and Rapid Kinetics in Lithium–Sulfur Batteries. *Adv. Energy Mater.* **2018**, *8*, 1800849.

(5) Chung, S.; Han, P.; Singhal, R.; Kalra, V. Electrochemically Stable Rechargeable Lithium–Sulfur Batteries with a Microporous Carbon Nanofiber Filter for Polysulfide. *Adv. Energy Mater.* **2015**, *5*, 1500738.

(6) Yang, Y.; Zhang, J. Highly Stable Lithium–Sulfur Batteries Based on Laponite Nanosheet-Coated Celgard Separators. *Adv. Energy Mater.* **2018**, *8*, 1801778.

(7) Sun, J.; Sun, Y.; Pasta, M.; Zhou, G.; Li, Y.; Liu, W.; Xiong, F.; Cui, Y. Entrapment of Polysulfides by a Black-Phosphorus-Modified Separator for Lithium–Sulfur Batteries. *Adv. Mater*. **2016**, *28*, 9797.

(8) Do, V.; Deepika; Kim, M. S.; Kim, M. S.; Lee, K. R.; Cho, W. I. Carbon Nitride Phosphorus as an Effective Lithium Polysulfide Adsorbent for Lithium–Sulfur Batteries. *ACS Appl. Mater. Interfaces* **2019**, *11*, 11431.

(9) Ali, S.; Waqas, M.; Jing, X.; Chen, N.; Chen, D.; Xiong, J.; He, W. Carbon−Tungsten Disulfide Composite Bilayer Separator for High-Performance Lithium−Sulfur Batteries. *ACS Appl. Mater. Interfaces* **2018**, *10*, 39417.